Chapter 3

Proximity effects in graphene and ferromagnetic $CrBr_3$ van der Waals heterostructure

3.1 Introduction

Interfacial phenomenon via MPE is one of the most essential phenomena in view of designing 2D magnetic vdW heterostructures [1]. In general, MPE is realized when two dissimilar materials of different lattice arrangement are coupled together to provide advanced functionalities [2, 3]. The impact of MPE results in modification of their properties and leads to variation of interfacial exchange coupling across the interface [4]. Till date, MPE has been investigated via exchange coupling between non-magnetic and magnetic substrates [5], and non-magnetic bilayer systems [6]. In these cases, it becomes challenging task to develop long-range magnetic ordering [7] and the induction of magnetic moment by the substrate *via* proximity effect in non-magnetic material has limited effects on charge and spin-based transport properties [8]. Alongside MPE, vdW heterostructures leverages with incorporation of external perturbation like strain [9], electric-field [10,11] and magnetic field [12] for their feasibility in engineering novel device. Graphene-based heterostructures have been explored previously by combining graphene with hexagonal boron nitride (hBN) for transistor applications [13] *via* modulating gate voltage [14] and ballistic transport in ambient conditions [15]. Robust exchange interactions have been demonstrated theoretically, where valley splitting is observed in graphene-bismuth ferrite (BFO) heterostructure [16]. Graphene is one of the

S K Behera* M Bora* S S P Chowdhury and P Deb, *Proximity effects in graphene and ferromagnetic $CrBr_3$ van der Waals heterostructures.* Phys. Chem. Chem. Phys., 21:25788, 2019.

ideal systems for nanospintronic applications due to its suitability in high electron mobility and long spin relaxation length [17]. The spin in graphene can be tuned *via* inducing local magnetic moment, electric field and strain to achieve advanced functionality in the material. Thus, the concept of spin injection into graphene by proximity effect is an interesting and emerging field of research. However, a basic challenge lies in the development of ways to externally tune (i.e., gating) the transmission of spin (i.e. spin-polarization) currents at room temperature, in view of designing spin logics. The growth of graphene on magnetic metallic substrates has been reported as a route to tailor graphene spin properties [18]. Therefore, magnetic conducting substrates fundamentally limit the design of novel types of spin devices by naturally short-circuiting the graphene layer. In this regard, 2D magnetic material and low-power spintronic devices offers current research opportunities with inherent long-range magnetic order in atomically thin crystals [19]. As a result, 2D layered magnetic materials can provide an efficient platform for spin control in the non-magnetic layer via MPE when integrated with other 2D materials for vdW heterostructures [16]. This implies new opportunities *via* introduction of magnetic insulators to induce magnetism in graphene by proximity effect in designed vdW heterostructures. However, the possibilities are limited in spintronics due to the absence of magnetic ordering and weak spin–orbit coupling.

The lacunas in graphene lead tremendous efforts to extrinsically induce local magnetic moments by various traditional methods like doping or introducing magnetic material [20], defect engineering [21], or introducing a magnetic substrate on which the graphene layer is stacked [22]. The graphene layer with a magnetic substrate is promising but it has limitations in establishing strong magnetic ordering and intrinsic moments induced by the substrate [7]. These limitations have enabled the exploration of possibilities in other 2D crystals such as chromium trihalides ($CrBr_3$) with intrinsic magnetic moments and band gap ranges (1–2.6 eV) [9, 23]. The 2D ferromagnetic semiconductor combined

with graphene to form magnetic heterostructure will be superior in proximity as well as electric field modulations, which are generally used as perturbative effects to vary the electronic properties of the 2D heterolayer system. The motivation behind the present work emerged from the successful experimental realization of the Gr-$CrBr_3$ heterostructure [24]. Herein, we investigate the MPE in a lattice-matched vdW heterostructure formed by a ferromagnet monolayer (i.e., $CrBr_3$) and a semimetal monolayer (i.e., graphene). This report helps in triggering the idea of exploring the external perturbative effects on the functionalities of the Gr–$CrBr_3$ heterostructure. It is observed that miniband splitting and spin polarization occurs in the electronic structure of graphene via the magnetic proximity effect induced by keeping the ferromagnetic $CrBr_3$ in the locus of 3.77 Å. In this chapter, we discuss the use of an *ab initio* density functional theory (DFT) simulation on the Gr–$CrBr_3$ heterostructure. Our results reveal the magnetic moment remains invariant in the monolayer $CrBr_3$ system, but a notable enhancement of 8% is observed in the hetero-bilayer system. Also, the interfacial polarization effect is found to be predominant in the Gr–$CrBr_3$ heterostructure. The electric-field tuning of the miniband splitting and ballistic transmission is observed in the Gr–$CrBr_3$ heterolayer using MPE, which makes the heterostructure system suitable for fabricating future nanoscale devices.

3.2 Model and Computational details

Theoretical calculations are conducted within the framework of *ab initio* DFT calculation by employing QE [25] software package, which uses the plane wave basis sets for computation and PAW [26] pseudopotential to describe the electron-core interaction in Gr-$CrBr_3$ heterostructure. The X_C energy is estimated by using GGA [27] within the PBE framework for the said heterostructure. The weak vdW interactions between Gr-$CrBr_3$ monolayers is considered using DFT-D2 method as implemented by Grimme [28], with vdWs radius of 2.744 Å, 2.952 Å and 3.305 Å for C, Cr and Br, respectively. The Hellmann-Feynman forces that act on the ions have been minimized to 0.01 eV

$Å^{-1}$ in the system to relax the structure. The interplanar distance between Gr-$CrBr_3$ monolayers is kept fixed at 3.77 Å with a strain of 1.8%. The vacuum of 20 Å is considered along the Z-direction to minimize the possible interactions of the periodic unit cell. The Kohn–Sham orbitals are expanded using the plane-wave basis set for which 680 eV of cut-off energy is used. Within the scheme of Monkhorst and Pack for the integrations in the Brillouin zone, a k-point grid of 9 x 9 x 1 has been followed in the self-consistent calculations [29]. The total energy of the system has been calculated with an accuracy of 10^{-8} eV by following the Davison method for iterative diagonalization of density matrices. For non-self-consistent calculations, a much denser k-point grid of 27 x 27 x 1 has been used for better accuracy in the results. A path consisting of highly symmetric k-points M–Γ–K–M has been used in the band structure calculations.

We consider the scattering formalism of PWCOND [30] module of QE code to perform the transmission coefficient calculations, which is based on *ab initio* DFT calculation. Here, the quantum-mechanical scattering channel is fixed and simulated to find the reflection (r_{ij}) and transmission (t_{ij}) amplitudes for electron waves (j) propagating towards the right direction from the left. Meanwhile, the total transmission at the Fermi energy is given as, $T(E_F) = \sum_{ij} |t_{ij}(E_F)|^2$, which is used later to obtain the linear ballistic conductance (G) *via* Landauer-Buttiker formula, $G=(e^2/h)T(E_F)$ implementing non-equilibrium Green's function (NEGF) in the calculation. The transmission spectra and associated parameters such as transmission eigen states and transmission pathways are simulated using self-consistent NEGF method.

3.3 Result and Discussions

3.3.1 Ground state Optimization

The ground state energy and corresponding interlayer distances were obtained by utilizing the surface atomic structure optimization via the Feynman-Hellman theorem [31]. Computationally, this is understood by Broyden-Fletcher-

Goldfarb-Shanno (BFGS) algorithm. The minimum energy configuration for heterostructure system is obtained when ferromagnetic ordering is considered. The atomic configurations are shown in Figure 3.1. The interlayer distance between graphene and $CrBr_3$ is 3.77 Å and interlayer interaction is considered as vdW type. Total energy was optimized as a function of interplanar distance as shown in Figure 3.1(b) to fix the optimal interplanar spacing for close proximity coupling between graphene and $CrBr_3$ incorporating dispersion correction [32]. Dispersion correction has been incorporated considering the bonding suitability of the $CrBr_3$ layer with graphene sheet to exactly obtain the total energy value with respect to interplanar spacing. To realize graphene sheets on the metal system as a heterostructure material, the junction resistance stemming from the metal–graphene interface must be understood and minimized during geometry optimization along with dispersion corrections on the van der Waals interacting system. In this calculation, we compiled the results to understand the metal–graphene heterostructure geometries to form a stable structure. This resistance plays a major role in controlling the electron transmission across the channel to realize the transmission properties of the system. Although the in-built resistance of the graphene sheet itself is also an important factor for a specific application, achieving the optimum resistivity value does not necessarily yield the desired device performance unless the junction in-built resistance is properly controlled and minimized during geometry optimization. Thus, the effects of bonding suitability and in-built resistance have been considered as prime dispersion parameters of Cr metal during the optimization process. Figure 3.1(d) refers the first Brillouin zone of hexagonal lattice considered for the ground state optimization of Gr-$CrBr_3$ heterostructure system.

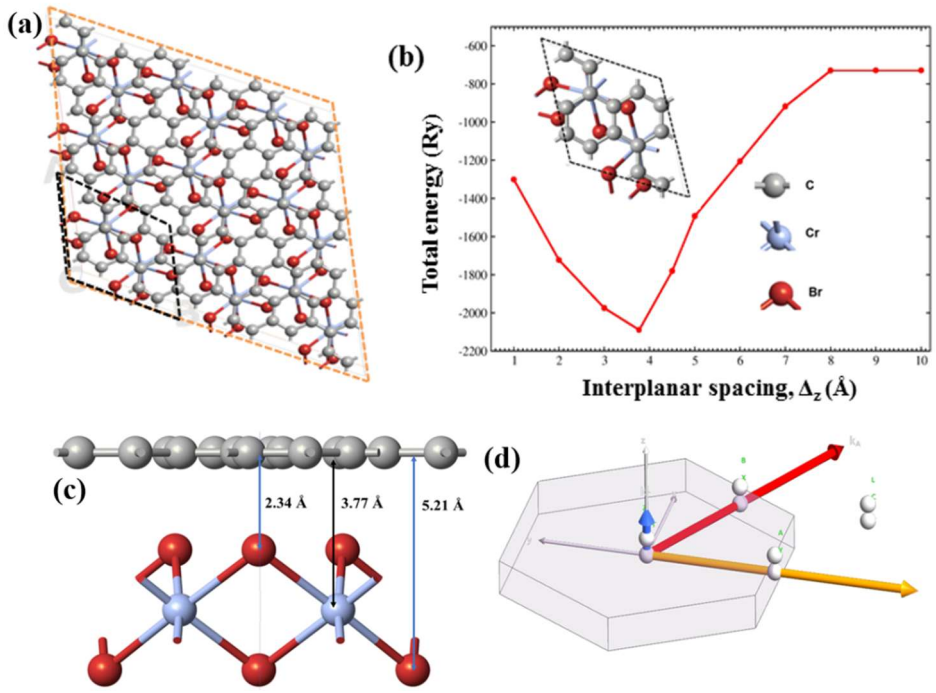

Figure 3.1: (a) Atomic configuration of Gr-$CrBr_3$ vdW heterolayer showing the top view of the supercell. (b) Variation of total energy with respect to interplanar spacing with dispersion correction (inset shows a unit cell of the heterostructure system). (c) Side view of Gr-$CrBr_3$ unit cell. The grey, blue and red balls describe C, Cr and Br atoms, respectively. (d) First Brillouin zone of Gr-$CrBr_3$ heterostructure system.

3.3.2 Electronic Structure

Electronic band structure of Gr-$CrBr_3$ heterostructure is plotted at zero bias, as shown in Figure 3.2(a). The spin-polarized electronic band structure observes a semiconducting nature in spin-up states and Dirac cone at K-point in spin-down states, respectively. Hence, the heterostructure system has a distinctive semimetal-semiconductor associated characteristic due to the proximity interaction between graphene and $CrBr_3$ monolayers. The partial density of states (PDOS) has been analyzed to check the individual orbital contribution of Gr-$CrBr_3$ heterostructure. In Figure 3.2(b), the state of л-bond delocalization and strong hybridization of p-orbitals of carbon atoms are present in the heterostructure, whereas the conduction band is dominated by C-p orbitals

with weakly hybridized s-orbitals in both spin-up and spin-down directions. Figure 3.2(c) shows the conduction band is influenced by Cr-4d_{z^2} orbital having intense peaks for both spin-up and spin-down states. The hybridization of Cr-d orbital is higher in the heterostructure system.

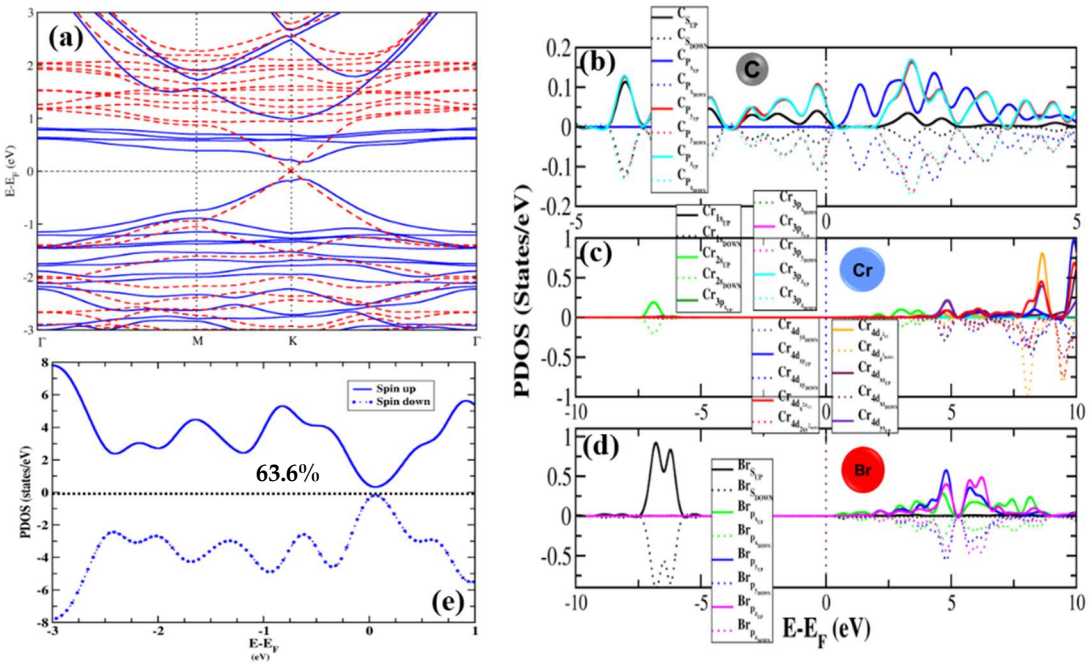

Figure 3.2: (a) Electronic band structure of the heterostructure in the absence of an external electric field. Blue continuous lines and red dashed lines show the up and down spin states, respectively. The calculated spin-polarized partial density of states (PDOS) of the Gr–$CrBr_3$ heterostructure: (b) carbon is shown as grey coloured ball, (c) chromium as blue coloured ball and (d) bromine as red coloured ball. (e) Total PDOS of the Gr–$CrBr_3$ heterostructure system with polarization percentage of up and down spin states.

Figure 3.2(d) illustrates the maximum contribution of the Br-p orbitals in the conduction band and intense peaks of the Br-s orbitals are observed for both spin-up and down directions in the valence band. s-Orbitals have almost pure element-independent character exhibiting a significant split energy gap from -5 eV to 0.1 eV. The contribution of Br-p orbitals is indicated by the intense peak in the conduction band and there is no significant role of s-orbitals in the conduction band. Therefore, it is seen that the p-orbitals of C and d-orbitals of

Cr are actively participating in the bonding of Gr-$CrBr_3$ heterostructure; p and d-orbitals are tuned when they come in close proximity. The spin-polarization effect (P) is explained by $P = \left|\frac{N_\uparrow(E_F)-N_\downarrow(E_F)}{N_\uparrow(E_F)+N_\downarrow(E_F)}\right|$, where $N_\uparrow(E_F)$ and $N_\downarrow(E_F)$ are the majority and minority spin channels at the Fermi region, respectively. The spin-polarization percentages obtained from the orbital resolved PDOS calculation for Gr-$CrBr_3$ were found to be 1.5%, 71.2% and 0.8% for carbon, chromium and bromine, respectively. It is obvious that the spin-polarization percentage for chromium will be significantly greater as compared to carbon and bromine due to the presence of inherent magnetic properties in chromium. A similar trend of spin-polarization was calculated for heterostructure systems averaging 63.6% (shown in Figure 3.2(e)), which clearly indicates the dynamic nature of all atomic orbital spins due to the proximity coupling between the semimetal graphene and ferromagnetic $CrBr_3$.

3.3.3 Charge and Spin density distribution

Charge and spin density describes the density of charges and spin are at a particular point. Figure 3.3(a) represents the charge density profile of Gr-$CrBr_3$ vdW heterostructure system. It is seen that the monolayer $CrBr_3$ has a semiconducting behaviour with a finite band gap, while the pristine monolayer graphene is a semimetal with zero band gap. It was observed that there was no adequate transfer of charge due to the vdW interaction between the two layers, but the distribution of charge on the surface of Gr–$CrBr_3$ heterostructure was found. The robustness of the proximity effect is mostly dependent on the orbital hybridization at the interface. The blue regions show the localization of electrons in the core. Moreover, the contribution of p and d-orbitals for C and Cr is also indicated by the PDOS, where C_p and Cr_d orbitals are more intense than the Br_p orbitals. This describes the delocalization of electrons identified from the green and yellow regions. Also, Figure 3.3(b) depicts the 2D mapping of electron density distribution, where red and yellow signify the electron accumulation and dissipation. It was clearly observed that there was no

continuous charge transfer among the atoms of the two layers, whereas there was an arrangement of charges on the surface of the Gr–$CrBr_3$ heterostructure.

Moreover, the spin density distribution is also plotted alongside electron density distribution for clear understanding of charge density distribution map on the surface of Gr-$CrBr_3$ heterostructure. Figure 3.3(c) depicts the 3D mapping of the spin density distribution where the yellow colour depicts the dense spin-polarized states of chromium atoms and cyan represents bromine with less dense spin-polarized states. This can also be corroborated by the 2D mapping of the spin density distribution (shown in Figure 3.3(d)) where the intense red colour signifies the dense spin-polarized state of the chromium atom. The cyan colour shows that the less spin-polarized state of bromine can be observed. Moreover, the spin-polarized percentage of Cr, C and Br can also be corroborated by the PDOS (shown in Figure 3.2(e)). The magnetic ordering in the heterostructure was found to be ferromagnetic in ground state with magnetic moment of 3.47 μ_B per cell. Moreover, the magnetic moment of the $CrBr_3$ monolayer was found to be 3.39 μ_B per cell with an increment of 39% as compared to the bulk counterpart value of 3.00 μ_B per cell [33] at zero external electric field. There was an increment in the magnetic moment of up to 8% in the heterostructure as compared to monolayer $CrBr_3$, indicating the magnetic proximity effect.

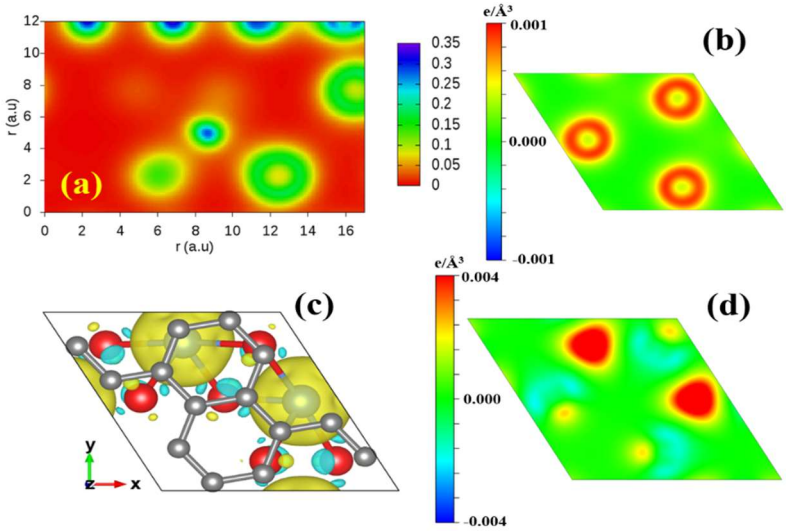

Figure 3.3: (a) Charge density profile for Gr-$CrBr_3$ heterolayer. (b) 2D profile of electron density map with the isosurface value of 0.001 e/Å^3 for the heterostructure. The positive and negative values in the color bar represent the accumulation and dissipation of charge, respectively. (c and d) Top-view of Gr-$CrBr_3$ heterostructure showing 3D and 2D mapping of spin density distribution with the isosurface value of 0.004 e/Å^3, respectively. The positive and negative values in color bar represent spin-polarized states.

3.3.4 Modulation of electronic structure with applied electric field

It was observed that there is a fluctuation in the split-off energy gap with respect to the bias voltage from 0 to $\pm$0.5 V Å^{-1} is shown in Figure 3.4(a). Thus, distinct nonlinearity is marked in this biasing, leading to interlayer polarization. Similarly, a decreasing trend (or increasing trend) was observed on increasing the field in reverse (or positive) bias from 0 to -0.5 (or +0.5) V Å^{-1}, indicating attractive (or repulsive) forces due to the interlayer polarization. The closing of the energy gap marks the tendency of variation in the direction of the reverse electric field, which is opposite to the in-built electric-field effect and can modulate the charge transport at the interface. Meanwhile, the mixed (i.e., linear and nonlinear) behaviour supports the investigation of the charge transmission spectra *via* ballistic transport calculations to realize the proximity effect in heterostructure and the role of the interlayer polarization. The

modulation in the Fermi energy level has been plotted against the applied field in both directions to have a comparative understanding (shown in Figure 3.5(b)). In the heterostructure, it was observed that non-linearity is present in both forward and reverse bias, enhancing the nonlinearity factor. As a result, the edge polarization is effective to form collective interlayer polarization. The split-off energy level of the heterostructure is shown as the band structure plot at 0 V $Å^{-1}$ (shown in Figure 3.5(c)). As the magnetic moment (3.39 μ_B per cell) remains invariant for the $CrBr_3$ monolayer with biasing, a minor distinct fluctuation ($\pm$0.06 μ_B per cell) in the moment value (3.47 μ_B per cell) was observed in the case of the heterostructure (shown in figure 3.4)

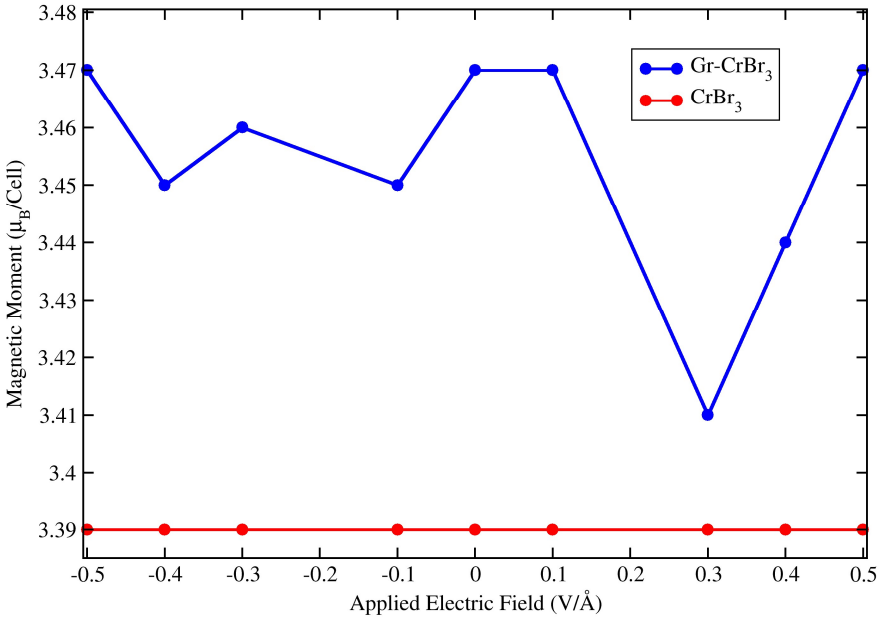

Figure 3.4: The variation of magnetic moment value for Gr-$CrBr_3$ heterostructure as well as for $CrBr_3$ monolayer as a function of applied electric field in 0 to $\pm$0.5 V/Å.

In the case of a metal, the effect of electrostatic screening is intrinsically controlled by the spin-dependent screening in the ferromagnetic content, which is of quantum mechanical origin [34] as shown in Figure 3.5(d) for the semimetal–ferromagnet heterojunction interface. The applied electrostatic field is screened from the interior of the Cr atom by the induced surface charges of

both spin (up and down) projections. However, the induced surface charge shows asymmetric majority and minority-spin contributions, leading to changes in the surface electronic and magnetic properties of the heterosystem. The relative amounts of these charge contributions have a quantum mechanical origin depending on the spin polarization of PDOS at the Fermi energy level. In Figure 3.5(d), the quantitative results of the charge distributions clearly demonstrate that the charge transfer in partial regions, especially for the several peaks and valleys, is significantly enhanced under a field of 0.5 V $Å^{-1}$. Reverse biasing of -0.5 V $Å^{-1}$ also enhances the charge transfer in most orbital regions, compared with the case of 0 V$Å^{-1}$. Here, the spin-dependent screening in C atoms of the graphene layer is negligible as compared to the Cr and Br atomic layers. This seems to imply that electric field gating fails to modify the spin polarization in a non-magnetic region, leading to a minute fluctuation in the induced magnetization values with respect to the biasing field in the heterostructure interface. Thus, the overall spin polarization to 63.6% in the heterostructure system and minor fluctuation in the moment value clearly show the active presence of magnetic proximity coupling at the heterojunction. Furthermore, proximity coupling can be considered as an external perturbation, which can play an important role in realizing the interfacial ballistic transport behaviour of the present heterostructure system.

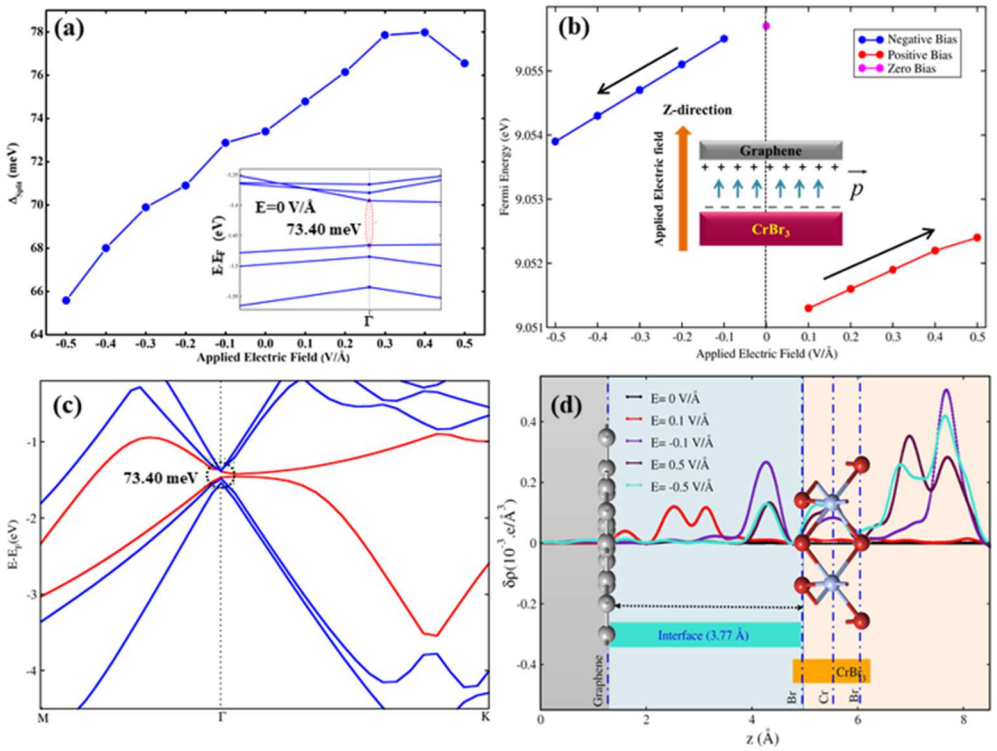

Figure 3.5: (a) The variation in the split-off energy as a function of the field of the heterostructure (inset shows the zoomed version of the energy split-off gap 73.40 meV at 0 V Å^{-1} field). (b) Variation in the Fermi energy due to the biasing via the external electric field in the range -0.5 to +0.5 V Å^{-1}. The schematic of the interfacial polarization is shown as the inset of (b) under biasing. (c) The energy split-off band structure at 0 VÅ^{-1} field. (d) Induced electrostatic charge density, δρ for the Gr–$CrBr_3$ heterostructure at different bias voltages for negative charge (-q) values. The atomic highlights of the Gr–$CrBr_3$ interface are shown as dotted vertical blue lines to note the unbalanced formation of electric dipole moments between graphene (C atom) and $CrBr_3$ (Cr and Br atoms) in accord with the number of atomic layers used to form the heterostructure.

3.3.5 Ballistic transport behaviour

The calculated transmission spectrum with respect to Fermi energy for the heterostructure is plotted as shown in Figure 3.5 (a). To understand the spin transport behaviour at the interface of the heterostructure, the lead-free transport property has been calculated *via* the NEGF process. Significant step-

like transmission spectra have been observed from the valence band to the conduction band in the heterostructure. Broad peaks near the transmission coefficient of ~6 have been observed in the conduction band in the energy window of 7.2–8.8 eV, which is due to the presence of strongly hybridized C-л states exhibited by graphene. As the C-p orbital is close enough to the $CrBr_3$ monolayer, we get the transmission coefficient T(E) > 2. Moreover, zero transmission coefficients have been noticed in certain energy windows (2.09–3.3 eV, 4.3–5.1 eV and 6.9–7.2 eV), which are due to no coupling effect with the leads. Although the energies of the electrons between p and d-orbitals are same, there might be a blockade of spins due to the absence of leads. As such, sudden drop in T(E) can be seen in small energy intervals.

Transmission spectra have been plotted with the change in the electric field in the forward and reverse bias (shown in Figure 3.5(b)). The energy intervals observed in the unbiased transmission spectrum are (0.39–2.13 eV), (3.26–4.32 eV) and (5.13–6.9 eV), which were found to be shifted and merged to the lower energy window region in the presence of an electric field in the forward (0.5 V $Å^{-1}$) and reverse (-0.5 V $Å^{-1}$) directions. It was observed that few intense and few narrow peaks were present in the spectrum, which supports that the ballistic transmission is controlled through the channel with the change in electric field, unlike the unbiased transmission spectrum that is suitable for field-effect transistor device application. It was observed that slight modulation occurred in the spectrum with respect to the bias voltage and the transmission spectrum remained mostly unchanged. The flow of the ballistically generated spins was checked from source to drain through the channel of the heterostructure. The spins generated from the source and detected in the drain clearly signify the switch ON state; otherwise, if the spins are scattered, it signifies the switch OFF state. Therefore, gating is important to trigger an effective electric field that arises due to the confinement of the transport channel and electrostatic screening in the heterostructure interface. This consistent nature of the spectrum supports the control of the interfacial polarization effect and flow

continuity along the channel due to the active proximity coupling leading to its suitability in designing single-gate field-effect transistor (SG-FET) devices as shown in Figure 3.6(e).

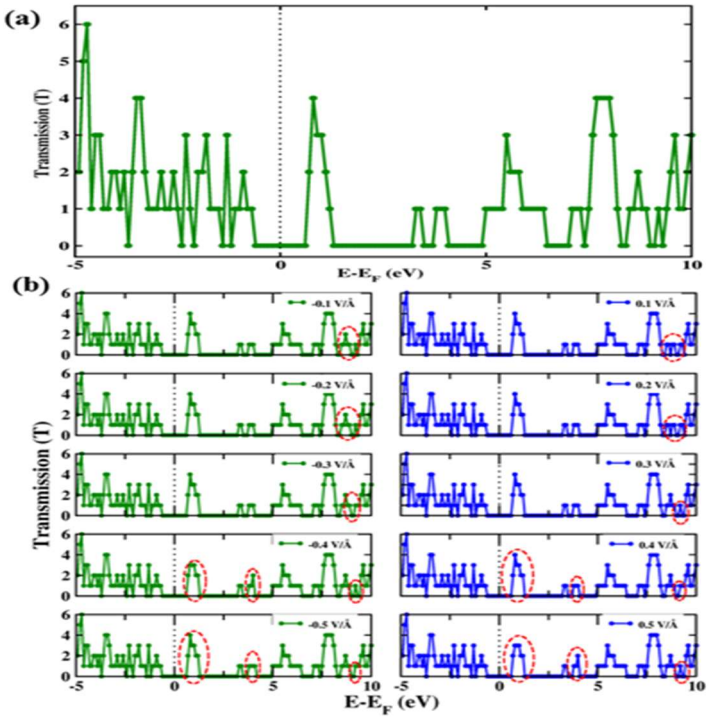

Figure 3.6: (a) The transmission coefficient calculation for the Gr-$CrBr_3$ vdW heterostructure at 0 $VÅ^{-1}$. (b) Field-induced transmission spectrum of the heterostructure in the forward and reverse directions. Minor changes in the spectrum are marked using red dotted ellipses.

3.3.6 Single-gate Field-effect transistor device model

The inclusion of the semimetallic graphene layer with $CrBr_3$ exerted a staggered potential on the $CrBr_3$ interface at a finite distance due to which the electron density and charge distribution were modulated in the heterolayer system. To facilitate a clear realization regarding these interface polarization phenomena, the Fermi energy diagram has been demonstrated schematically in Figure 3.6(a) and (b). A perpendicular electric field has been applied to the heterosystem in both the positive and negative directions of the Z-axis, while the magnetic ordering is imposed along the X-axis following the ferromagnetic ordering. The

field variation is considered in VÅ^{-1} along the specified direction as shown in Figure 3(c) and (d). Here, in the present case of calculations, the application of the perpendicular external electric field, which causes a redistribution of charges, is not likely to lead to any structural changes in the surface atoms of the heterolayer system as previously observed in silicone-based hetero layers [35]. We display the development of SG-FET prototype with switch on-off ratio taking into account the model Gr-$CrBr_3$ bilayer system as shown in Figure 3.6(e). Gr–$CrBr_3$ is sandwiched between two electrodes (source and drain) in the central region. The gate is placed above the central region so that the flow of electrons is possible through the channel from source to drain when applying an external electric field.

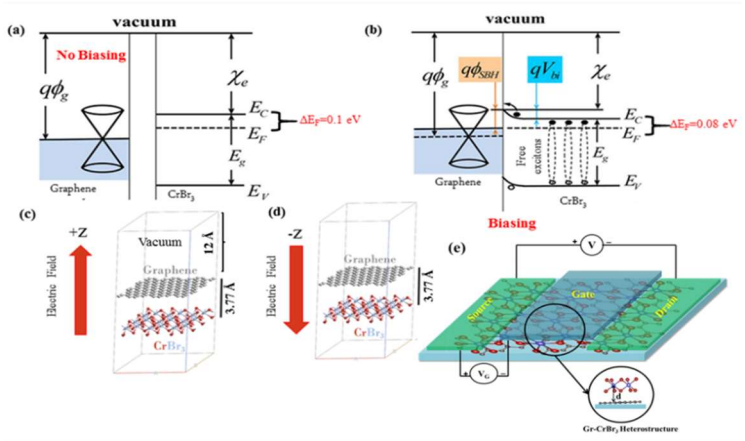

Figure 3.7: Schematic representation of the Gr–$CrBr_3$ hetero-bilayer (a) without and (b) with biasing. Application of an external electric field in (c) positive (+Z direction) and (d) negative (-Z direction) bias; (e) the proposed device model for the SG-FET device.

3.4 Concluding Remarks

In conclusion, we investigated first-principles based simulations showing that the proximity of a ferromagnetic insulator, $CrBr_3$, will induce strong spin polarization of graphene orbitals. The $CrBr_3$ substrate was found to break the bipartite lattice of graphene into six inequivalent sublattices, resulting in variable spin polarizations on the new graphene sublattices with an average

spin polarization of about 63.6%. Simultaneously, a miniband split-off energy gap developed with a splitting of 73.40 meV, together with a magnetic moment of 3.47 μ_B per cell in the heterostructure, 8% larger than the monolayer $CrBr_3$ sheet. Taking into account the effect of proximity coupling at the interplanar distance of 3.77 Å in forming the heterolayer, we observed the miniband state localized periodically in the interface of the heterostructure. The magnetic proximity effect in the heterojunction was reflected in the spin splitting of the miniband in the electronic band structure, which provides a platform for studying the strong proximity correlation effect. An applied perpendicular electric field tunes the miniband spin splitting and transmission spectrum. Furthermore, the interfacial polarization effect activates electrostatic screening reinforcing the transmission in the heterolayer. These theoretical results deserve further experimental realization of the spin splitting effect and the field-dependent energy gap tuning in graphene-based magnetic heterostructures for novel nanoscale devices.

References

[1] Hauser, J. J. Magnetic Proximity effect. *Physical Review*, 187:580, 1969.

[2] White, R. M. and Friedman, D. J. Theory of the magnetic proximity effect. *Journal of Magnetism and Magnetic Materials*, 49:117, 1985.

[3] Manna, P. K. and Yusuf, S. M. Two interface effects: Exchange bias and magnetic proximity. *Physics Reports*, 535:61, 2014.

[4] Vasili, H. B., Gamino, M., Gazquez, J., Sanchez, F., Valvidares, M., Gargiani, P., Pellegrin, E. and Fontcuberta J. Magnetoresistance in Hybrid Pt/$CoFe_2O_4$ Bilayers Controlled by Competing Spin Accumulation and Interfacial Chemical Reconstruction. *ACS Applied Materials & Interfaces*, 10:12031, 2018.

[5] Li, Y., Wang, J., Zhou, B., Wang, F., Miao, Y., Wei, J., Zhang, B. and Zhang, K. Tunable interlayer coupling and Schottky barrier in graphene and Janus

MoSSe heterostructures by applying an external field. *Physical Chemistry Chemical Physics*, 20:24109, 2018.

[6] Phuc, H. V., Hieu, N. N., Hoi, B. D. and Nguyen, C. V. Interlayer coupling and electric field tunable electronic properties and Schottky barrier in a graphene/bilayer-GaSe van der Waals heterostructure. *Physical Chemistry Chemical Physics*, 20:17899, 2018.

[7] Nair, R. R., Sepioni, M., Tsai, I. L., Lehtinen, O., Keinonen, J., Krasheninnikov, A. V., Thomson, T., Geim, A. K. and Grigorieva, I. V. Spin-half paramagnetism in graphene induced by points defects. *Nature Physics*, 8:199, 2012.

[8] Pi, K., Han, W., McCreary, K. M., Swartz, A. G., Li, Y. and Kawakami, R. K. Manipulation of Spin Transport in Graphene by Surface Chemical Doping. *Physical Review Letter*, 104:187201, 2010.

[9] Webster, L. and Yan, J. -Y. Strain-tunable magnetic anisotropy in monolayer $CrCl_3$, $CrBr_3$ and CrI_3. *Physical Review B*, 98:144411, 2018.

[10] Song, H. -D., Zhu, P. -F., Yang, X., Qin, M., Ren, Z., Duan, C. -G., Han, G., Liao, Z. -M. and Yu, D. Electrical control of magnetic proximity effect in a graphene/multiferroic heterostructure. *Applied Physics Letter*, 113:183101, 2018.

[11] Liu, X., Burton, J. D., Zhuravlev, M. Y. and Tsymbal, E. Y. Electric control of spin injection into a ferroelectric semiconductor. *Physical Review Letter*, 114:046601, 2015.

[12] Zhang, Y. Q., Sun, N. Y., Che, W. R., Li, X. L., Zhang, J. W., Shan, R., Zhu, Z. G. and Su, G. Manipulating effective spin orbit coupling based on proximity effect in magnetic bilayers. *Applied Physics Letter*, 107:082404, 2015.

[13] Behera, S. K. and Deb, P. Controlling the bandgap in graphene/h-BN heterostructures to realize electron mobility for high performing FETs. RSC Advances, 7:31393, 2017.

[14] Lazic, P., Belashchenko, K. D. and Zutic, I. Effective gating and tunable magnetic proximity effects in two-dimensional heterostructures. *Physical Review B*, 93:241401(R), 2016.

[15] Cardoso, C., Soriano, D., Garcia-Martinez, N. A. and Fernandez-Rossier, J. van der Waals spin valves. *Physical Review Letter*, 121:067701, 2018.

[16] Qiao, Z., Ren, W., Chen, H., Bellaiche, L., Zhang, Z., MacDonald, A. H. and Niu, Q. Quantum anomalous Hall effect in Graphene proximity coupled to an antiferromagnetic insulator. *Physical Review Letter*, 112:116404, 2014.

[17] Chang, C. -Z., Zhao, W., Kim, D. Y., Zhang, H., Assaf, B. A., Heiman, D., Zhang, S. -C., Liu, C., Chan, M. H. W. and Moodera, J. S. High-precision realization of robust quantum anomalous Hall state in a hard ferromagnetic topological insulator. *Nature Materials*, 14(5):473, 2015.

[18] Rader, O., Varykhalov, A., Sanchez-Barriga, J., Marchenko, D., Rybkin, A. and Shikin, A. M. Is there a Rashba effect in Graphene on 3d Ferromagnets? *Physical Review Letter*, 102:057602, 2009.

[19] Burch, K. S., Mandrus, D. and Park, J. -G. Magnetism in two-dimensional van der Waals materials. *Nature*, 563:47, 2018.

[20] Fan, M., Wu, J., Yuan, J., Deng, L., Zhong, N., He, L., Cui, J., Wang, Z., Behera, S. K., Zhang, C., Lai, J., Jawdat, B. I., Vajtai, R., Deb, P., Huang, Y., Qian, J., Yang, J., Tour, J. M., Lou, J., Chu, C. W., Sun, D. and Ajayan, P. M. Doping nanoscale graphene domains improves magnetism in hexagonal boron nitride. *Advanced Materials*, 31:1805778, 2019.

[21] Gonzalez-Herrero, H., Gomez-Rodriguez, J. M., Mallet, P., Moaied, M., Palacios, J. J., Salgado, C., Ugeda, M. M., Veuillen, J. Y., Yndurain, F. and Brihuega, I. Atomic-scale control of graphene magnetism by using hydrogen atoms. *Science*, 352:437, 2016.

[22] Hallal, A., Ibrahim, F., Yang, H., Roche, S. and Chshiev, M. Tailoring magnetic insulator proximity effects in graphene: First-principles calculations. *2D Materials*, 4:025074, 2017.

[23] Zhang, H., Ning, Y., Yang, W., Zhang, J., Zhang, R. and Xu, X. Possible realization of the high-temperature and multichannel quantum anomalous Hall effect in graphene/$CrBr_3$ heterostructure under pressure. *Physical Chemistry Chemical Physics*, 21:17087, 2019.

[24] Ghazaryan, D., Greenaway, M. T., Wang, Z., Guarochico-Moreira, V. H., Vera-Marun, I. J., Yin, J., Liao, Y., Morozov, S. V., Kristanovski, O., Lichtenstein, A. I., Katsnelson, M. I., Withers, F., Mishchenko, A., Eaves, L., Geim, A. K., Novoselov, K. S. and Misra, A. Magnon-assisted tunnelling in van der Waals heterostructures based on $CrBr_3$. *Nature Electronics*, 1:344, 2018.

[25] Giannozzi, P., Baroni, S., Bonini, N., Calandra, M., Car, R., Cavazzoni, C., Ceresoli, D., Chiarotti, G. L., Cococcioni, M., Dabo, I., Corso, A. D., de Gironcoli, S., Fabris, S., Fratesi, G., Gebauer, R., Gerstmann, U., Gougoussis, C., Kokalj, A., Lazzeri, M., Martin-Samos, L., Marzari, N., Mauri, F., Mazzarello, R., Paolini, S., Pasquarello, A., Paulatto, L., Sbraccia, C., Scandolo, S., Sclauzero, G., Seitsonen, A. P., Smogunov, A., Umari, P., and Wentzcovitch, R. M. QUANTUM ESPRESSO: a modular and open-source software project for quantum simulations of materials. *Journal of Physics: Condensed Matter*, 21(39):395502, 2009.

[26] Blochl, P. E. Projector augmented-wave method. *Physical Review B*, 50:17953, 1994.

[27] Perdew, J. P., Burke, K. and Ernzerhof, M. Generalized gradient approximation made simple. *Physical Review Letter*, 77:3865, 1996.

[28] Grimme, S. Semiempirical GGA-type density functional constructed with a long-range dispersion correction. *Journal of Computational Chemistry*, 27(15):1787–1799, 2006.

[29] Tkatchenko, A. and Scheffler, M. Accurate molecular van der Waals interactions from ground-state electron density and free-atom reference data. *Physical Review Letter*, 102:073005, 2009.

[30] Smogunov, A., Corso, A. D. and Tosatti, E. Ballistic conductance of magnetic Co and Ni nanowires with ultrasoft pseudopotentials. *Physical Review B*, 70:045417, 2004.

[31] Feynman, R. P. Forces in molecules. *Physical Review*, 56:340, 1939.

[32] Pernal, K. Electron Correlation from the Adiabatic Connection for Multireference Wave Functions. *Physical Review Letter*, 120:013001, 2018.

[33] Dhillon, J. F., Kamimura, Jr. H. and Remeika, J. P. Magnetic Rotation of Visible Light by Ferromagnetic $CrBr_3$. *Physical Review Letter*, 9:161, 1962.

[34] Brovko, O. O., Farberovich, O. V. and Stepanyuk, V. S. Electric field for tuning quantum entanglement in supported clusters. Journal of Physics: Condensed Matter, 26:315010, 2014.

[35] Nigam, S., Gupta, S. K., Majumder, C. and Pandey, R. Modulation of band gap by an applied electric field in silicene-based hetero-bilayers. *Physical Chemistry Chemical Physics*, 17:11324, 2015.